Bioenergetic Profiles Diverge During Macrophage Polarization: Implications for the Interpretation of ^{18}F-FDG PET Imaging of Atherosclerosis

Sina Tavakoli[1], Debora Zamora[2,3], Sarah Ullevig[4], and Reto Asmis[1,2,4]

[1]Department of Radiology, University of Texas Health Science Center at San Antonio, San Antonio, Texas; [2]Department of Clinical Laboratory Sciences, University of Texas Health Science Center at San Antonio, San Antonio, Texas; [3]Department of Biology, Trinity University, San Antonio, San Antonio, Texas; and [4]Department of Biochemistry, University of Texas Health Science Center at San Antonio, San Antonio, Texas

Conventional cardiovascular imaging is invaluable for the assessment of late sequelae of atherosclerosis, such as diminished perfusion reserve and luminal stenosis. Molecular imaging provides complementary information about plaque composition and ongoing biologic processes in the vessel wall, allowing the early diagnosis and risk stratification of patients. Detection of enhanced glucose uptake, using ^{18}F-FDG PET, has been proposed as a noninvasive approach to track macrophage activation as a critical event in the development and progression of atherosclerosis. In this study, we determined the impact of macrophage polarization on glucose metabolism and oxidative phosphorylation. **Methods:** Murine peritoneal macrophages were incubated in the presence of interferon-γ (IFN-γ) plus tumor necrosis factor-α (TNF-α), lipopolysaccharide (LPS), or interleukin-4 (IL-4) to induce classic (M1 and M_{LPS}) or alternative (M2) polarization, respectively. Glucose uptake was measured using ^{3}H-deoxyglucose. Oxidative phosphorylation was evaluated using an extracellular flux analyzer. Mitochondrial DNA copy numbers were quantified by polymerase chain reaction. The expression of glucose transporter-1 (*Glut-1*), hexokinase-1 and -2 (*Hk-1* and *Hk-2,* respectively), mitochondrial transcription factor-1 (*Tfam*), and cytochrome c oxidase subunit I (*Cox-1*) was determined by quantitative reverse transcription polymerase chain reaction. **Results:** Stimulation of macrophages by LPS, but not polarization with either IFN-γ plus TNF-α (M1) or IL-4 (M2), resulted in a 2.5-fold increase in ^{3}H-deoxyglucose uptake. Enhanced glucose uptake by M_{LPS} macrophages paralleled the overexpression of rate-limiting proteins involved in transmembrane transport and intracellular trapping of glucose—that is, *Glut-1, Hk-1,* and *Hk-2*. Alternatively polarized M2 macrophages developed a markedly higher spare respiratory capacity than both nonpolarized and classically polarized M1 macrophages. M2 polarization was associated with a 4.6-fold increase in mitochondrial content of the cells, compared with nonpolarized macrophages. The expression of *Tfam,* a major regulator of mitochondrial biogenesis, and *Cox-1,* a critical component of respiratory chain, was significantly increased in M2 polarized macrophages. **Conclusion:** Polarization of macrophages induces distinct metabolic profiles with respect to glycolysis versus oxidative phosphorylation, with alternatively polarized macrophages shifting to mitochondria as their main source of adenosine triphosphate. Only M_{LPS}, but not M1 or M2 polarized macrophages, showed increased glucose uptake, suggesting that glucose metabolism is regulated independent of the polarization state and macrophage polarization may not be detectable by ^{18}F-FDG PET.

Key Words: macrophage polarization; glucose uptake; oxidative phosphorylation; ^{18}F-FDG; PET

Atherosclerosis is characterized by the continuous recruitment and accumulation of monocyte-derived macrophages in large- and medium-sized arteries. The pathologic and clinical manifestations of atherosclerosis are highly variable, ranging from chronic ischemic symptoms, caused by luminal stenosis and decreased perfusion reserve, to acute life-threatening complications, such as myocardial infarction, as a result of plaque rupture or ulceration (*1,2*). Therefore, stratifying risk, predicting the course of disease, and monitoring the response to therapeutic or preventive measures are important to establish an individualized approach to patient management (*1,2*). Currently, conventional or computed tomographic angiography and myocardial perfusion scintigraphy are the cornerstones of coronary atherosclerosis diagnosis. However, these modalities are limited to advanced stages of disease when significant luminal stenosis and reduced perfusion reserve have already occurred (*1,2*). Most acute myocardial events result from the rupture of plaques, which do not produce hemodynamically significant stenosis (*3*), further limiting the potential of conventional imaging techniques. These vulnerable plaques are rich in inflammatory cells, in particular macrophages, which contribute to plaque expansion and weakening of the supportive fibrous cap through expression of numerous cytokines, chemokines, and proteases predisposing the plaque to rupture (*1,2*). Therefore, there has been a growing interest in the development and validation of diagnostic approaches that specifically target ongoing cellular and molecular events occurring in the atherosclerotic vessel wall rather than assessment of their late consequences.

The widespread availability of ^{18}F-FDG as a Food and Drug Administration–approved radiopharmaceutical, and the safety concerns linked to other alternative imaging approaches (e.g., potential adverse biologic effects of novel targeting agents, limited

biodegradability of nanoparticles, and such), may explain why in vivo targeting of macrophages by PET superseded other molecular approaches in clinical imaging of atherosclerosis. Early ^{18}F-FDG–based PET imaging studies showed promising results in both the detection of inflammatory lesions and the response of these lesions to therapeutic interventions (4–8). However, some clinical studies failed to demonstrate a significant association between plaque inflammation and ^{18}F-FDG uptake (4,9), hindering the translation of experimental studies to the clinical practice. Additionally, a direct association between increased glucose uptake and specific macrophage functions or activation states has yet to be validated.

Macrophages are primarily glycolytic (10). At least 2 major polarization phenotypes of macrophages have been identified—that is, the proinflammatory (classic or M1) and the antiinflammatory (alternative or M2) polarization states. Macrophages play opposing functions in atherosclerosis and, within the vessel wall, may be involved in both the progression and the resolution of inflammation (11,12). It has been assumed that enhanced ^{18}F-FDG uptake in atherosclerotic lesions arises from inflammatory activation of macrophages (13) (i.e., polarization toward the M1 phenotype) and thus may be used to monitor inflammatory burden of plaque and progression or response to therapy. However, experimental data have been controversial.

In this study, we evaluated the bioenergetic profile of non-activated (M0) as well as classically (M1, interferon-γ [IFN-γ] plus tumor necrosis factor-α [TNF-α]) and alternatively (M2, interleukin-4 [IL-4]) polarized macrophages. Lipopolysaccharide (LPS) stimulation was used as an alternative method to induce an inflammatory macrophage phenotype (M$_{LPS}$). Our data show that glycolytic and oxidative phosphorylation profiles are distinct between different macrophage phenotypes and depend on both the polarization state and the specific stimulatory agents. However, glucose uptake was enhanced only in response to LPS stimulation. Our findings demonstrate that macrophage polarization is not necessarily associated with increased glucose uptake and thus may not be detected by ^{18}F-FDG PET imaging. Furthermore, the distinct metabolic profiles of M1 and M2 macrophages suggest distinct functions, responses, and fates of these macrophage subsets in response to the dynamic microenvironment of atherosclerotic plaques.

MATERIALS AND METHODS

Animals

C57BL/6J mice were obtained from The Jackson Laboratories, bred in-house, and fed a regular chow served as the source of primary peritoneal macrophages for cell culture studies. Experiments were performed according to regulations of the Animal Care and Use Committees of the University of Texas Health Science Center at San Antonio.

Cell Culture

Cell culture reagents were purchased from Gibco, unless otherwise specified. Resident peritoneal cells were harvested from mice euthanized by isoflurane and plated in RPMI-1640 medium, as previously described (14). After a 6-h incubation at 37°C, nonadherent cells were removed by washing 3 times with the medium. Adherent macrophages were cultured for 2 d in RPMI-1640 supplemented with 10% fetal bovine serum, 1 mM sodium pyruvate, 2 mM GlutaMAX, nonessential amino acids, and 20 mM N-(2-hydroxyethyl)piperazine-N′-(2-ethanesulfonic acid) buffer in the presence of IFN-γ plus TNF-α (PeproTech; 50 and 10 ng/mL, respectively) or LPS (Calbiochem; 10 ng/mL) to induce inflammatory phenotypes, M1 polarization and M$_{LPS}$, respectively. Alternative (M2) polarization was induced using IL-4 (PeproTech; 10 ng/mL) for the same duration. Macrophages that were grown in the absence of the above cytokines were considered nonpolarized or M0. The cell viability was greater than 95% as determined by Calcein AM (Invitrogen) staining (data not shown).

Glucose Uptake Assay

Macrophages were washed 3 times with phosphate-buffered saline and incubated for 15 min at 37°C with glucose and serum-free RPMI-1640 supplemented with pyruvate and nonessential amino acids. ^{3}H-2-deoxyglucose (2.22 GBq/μmol; American Radiolabeled Chemicals Inc.) was added to the culture medium at a specific activity of 37 kBq/mL, and cells were incubated for 30 min at 37°C. Subsequently, cells were washed 3 times with cold phosphate-buffered saline and lysed with 0.1 mM NaOH. ^{3}H-2-deoxyglucose uptake was determined in the lysates by liquid scintillation counting (LS 5000TD; Beckman Coulter) and normalized to the protein content as determined by bicinchoninic acid assay (Pierce). ^{3}H-2-deoxyglucose uptake for each sample is expressed relative to the uptake by nonpolarized macrophages.

Mitochondrial Bioenergetic Assay

Lymphocytes constitute most of the nonmacrophage population among resident peritoneal cells. To ensure a consistent cell density among the experiments (125,000 cells/well), we depleted lymphocytes from the peritoneal cell suspensions using mouse pan T (Thy1.2) and pan B (B220) Dynabeads (Invitrogen) for mitochondrial bioenergetics studies. Macrophages from 2–3 mice were pooled before plating and were subsequently polarized, as described above. One hour before the mitochondrial bioenergetic assay was performed, culture medium was replaced with serum- and bicarbonate-free RPMI-1640 (HyClone, SH40015-11) supplemented with 1 mM sodium pyruvate and nonessential amino acids. Cells were allowed to equilibrate for 1 h at 37°C. Subsequently, the oxygen consumption rate (OCR) and extracellular acidification rates (ECAR) were measured using a Seahorse Extracellular Flux (XF) Analyzer (Seahorse Bioscience) following the manufacturer's instructions. Basal OCR and ECAR as well as response to sequential incubation with the mitochondrial inhibitors oligomycin (1.45 μM), carbonyl cyanide-p-trifluoromethoxyphenylhydrazone (FCCP, 1.45 μM), and rotenone (1 μM) were recorded. Oligomycin is an adenosine triphosphate (ATP) synthase inhibitor and differentiates oxygen consumption that is used for ATP synthesis from proton leak across the inner mitochondrial membrane (15). FCCP uncouples the proton transport from ATP synthesis, resulting in the maximal oxygen consumption without mitochondrial ATP generation, reflecting the maximal respiratory capacity of the cells. The difference between maximal OCR (after addition of FCCP) and basal OCR is the mitochondrial spare respiratory capacity (15). Rotenone inhibits mitochondrial complex I and interferes with the use of nicotinamide adenine dinucleotide (NADH) for ATP synthesis. The rotenone-insensitive OCR reflects nonmitochondrial respiration (15). On completion of the experiments, cells were lysed, and their DNA contents were measured using the PicoGreen reagent (Invitrogen). OCR and ECAR data were normalized to the DNA content.

Nitric Oxide (NO) Production Assay

Intracellular NO production was analyzed by incubating adherent cells for 30 min with 1 μM 4-amino-5-methylamino-2′,7′-difluorescein (DAF-FM) diacetate (Molecular Probes). Cell were harvested, washed with phosphate-buffered saline, and subsequently analyzed by flow cytometry using a FACSCalibur flow cytometer (Becton Dickinson). Data were analyzed using FlowJo software (Tree Star Inc.). Mean fluorescence intensity values were calculated, and values are expressed as fold change relative to NO production by M0 macrophages.

Gene Expression Assay

Total RNA was isolated from cells using Trizol reagent (Invitrogen). Reverse transcription was performed using a QuantiTect Reverse Transcription Kit, according to the manufacturer's instructions. Quantitative reverse transcription polymerase chain reaction (qRT-PCR) was performed on complementary DNA samples in triplicate using Taqman gene expression assays (Invitrogen) and a real-time PCR system (model 7900HT; Applied Biosystems). The following primers were used: nitric oxide synthase-2 (*Nos-2,* Mm00440502_m1), *Tnf-α* (Mm00443258_m1), found in inflammatory zone 1 (*Fizz-1,* Mm00445109_m1), arginase-1 (*Arg-1,* Mm00475988_m1), chemokine (C-X-C motif) ligand 9 (*Cxcl-9,* Mm00434946_m1), glucose transporter-1 (*Glut-1,* Mm00441480_m1), hexokinase-1 (*Hk-1,* Mm00439344_m1), hexokinase-2 (*Hk-2,* Mm00443385_m1), mitochondrial transcription factor 1 (*Tfam,* Mm00447485_m1), cytochrome c oxidase subunit I (*Cox-1,* Mm04225243_g1), and hypoxanthine guanine phosphoribosyltransferase (*Hprt,* Mm01545399_m1). Amplification data were analyzed using SDS2.4 software (Applied Biosystems), and gene expression levels were normalized to *Hprt* as the housekeeping gene.

Mitochondrial DNA (mtDNA) Copy Number

mtDNA copy number was measured using quantitative PCR, as described previously (*16*). Cells were harvested in the lysis buffer (10 mM Tris–HCl, 1 mM ethylenediaminetetraacetic acid [EDTA] and 0.1% sodium dodecyl sulfate [SDS]) and incubated with proteinase K at 55°C for 2 h. DNA was extracted using phenol:chloroform:isoamyl alcohol (25:4:1), followed by chloroform phase separation. DNA was subsequently precipitated using sodium acetate–isopropanol and washed with 75% ethanol. After resuspension in H_2O, total DNA concentration was measured using a Nanodrop 1000 spectrophotometer (Thermo Scientific). Quantitative PCR amplification of cytochrome c oxidase subunit I (forward primer sequence: 5′-TGCTAGCCG-CAGGCATTAC-3′; reverse primer: 5′-GGGTGCCCAAAGAATCA-GAAC-3′) and NADH dehydrogenase ubiquinone flavoprotein 1 (forward primer: 5′-CTTCCCCACTGGCCTCAAG-3′; reverse primer: 5′-CCAAAACCCAGTGATCCAGC-3′), as mtDNA and nuclear DNA (nDNA) encoded genes, respectively, was performed in triplicate using SYBR Green PCR Master Mix (Invitrogen) (*16*). The ratio of mtDNA to nDNA was calculated as a marker of macrophage content of the cells.

Statistical Analysis

Statistical analyses were performed using Sigma Stat 12.0 (Systat Software, Inc.). Data are expressed as mean ± SD of at least 3 experiments. ANOVA, followed by the Tukey post hoc test, was used to compare the mean values between multiple groups. A *P* value of less than 0.05 was considered statistically significant.

RESULTS

Ex Vivo Polarization of Murine Peritoneal Macrophages

To examine whether the activation state of macrophages alters their bioenergetics and substrate preference, we chose 3 frequently used models of macrophage polarization: IFN-γ plus TNF-α (M1) or LPS (M_{LPS}) stimulation to generate inflammatory macrophages and IL-4 stimulation as a model of alternative or M2 polarization. Untreated peritoneal cells were considered nonpolarized or M0. Polarization of murine peritoneal macrophages was confirmed by qRT-PCR using a panel of established markers of classic (*Nos-2*, *Tnf-α*, *Cxcl-9*) and alternative (*Arg-1*, *Fizz-1*) macrophage activation (Fig. 1). M1 macrophages showed significantly higher expression of *Nos-2*, *Tnf-α,* and *Cxcl-9* than M0 and M2 polarized cells. In contrast, M2 polarization resulted in a substantial increase in the expression of *Arg-1* and *Fizz-1*. Similar to M1 macrophages, M_{LPS} macrophages demonstrated a marked induction of *Nos-2* and *Tnf-α,* consistent with a proinflammatory phenotype. However, the expression of an alternative polarization marker, *Arg-1,* was also highly increased in M_{LPS} macrophages, though significantly less than the expression level by M2 polarized macrophages, which distinguished LPS stimulation from IFN-γ plus TNF-α–induced classic polarization. The concomitant induction of M1 markers with *Arg-1* overexpression is consistent with the acquisition of some M2-like phenotypes, associated with endotoxin tolerance induced by long-term exposure to LPS (*17,18*). To confirm that IFN-γ plus TNF-α treatment induces a classically polarized macrophage phenotype, we measured intracellular NO production.
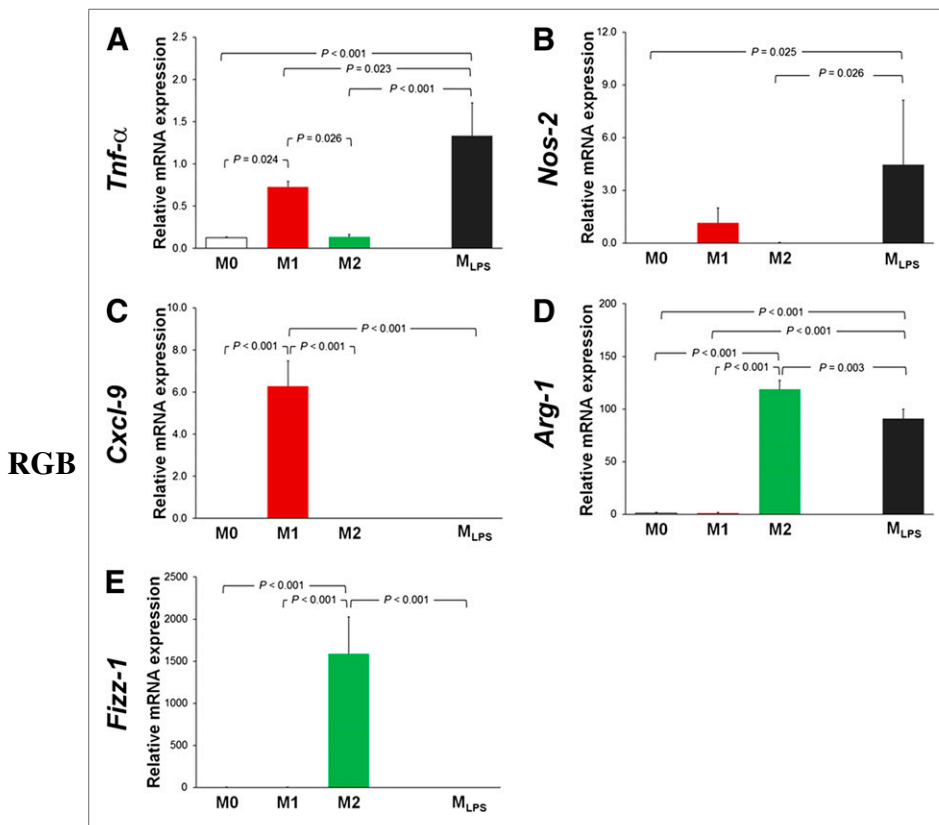
[Fig. 1]

RGB

FIGURE 1. Characterization of polarized peritoneal macrophages. qRT-PCR confirms distinctive polarization states of macrophages in our ex vivo system. M1 and M_{LPS} polarization phenotypes were verified by overexpression of *Nos-2* and *Tnf-α*. M2 polarization phenotype was characterized by increased expression of *Arg-1* and *Fizz-1*. LPS treatment induced expression of *Arg-1,* consistent with the development of an endotoxin-tolerance phenotype. Data are expressed relative to expression of housekeeping gene *Hprt* (*n* = 3–4). mRNA = messenger RNA.
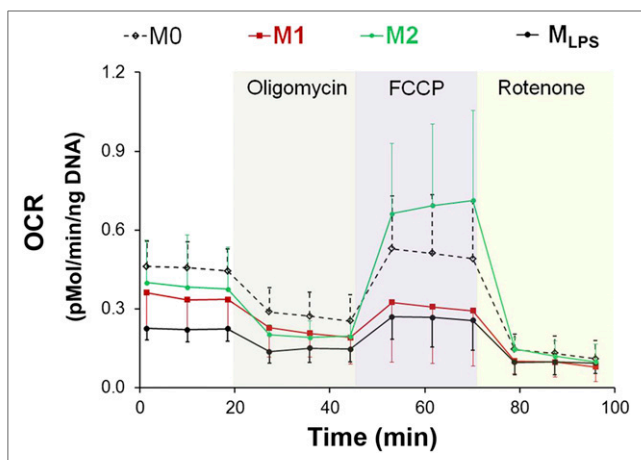
Using the NO-sensitive fluorescent dye DAF-FM, we demonstrated a 2.6-fold increase in fluorescence in M1 macrophages compared with M0 macrophages (Supplemental Fig. 1; supplemental materials are available at http://jnm.snmjournals.org). Interestingly, intracellular NO production was not elevated in M_{LPS} macrophages, compared with M0 macrophages. One likely explanation for this result might be found in the competition for the substrate, arginine, between arginase and NO synthase, because both enzymes are induced by long-term LPS treatment. The distinct expression patterns of the marker genes and NO production obtained in our ex vivo system confirm that each of the 3 activation conditions generated a unique macrophage polarization state.

Enhanced Glucose Uptake in M_{LPS} Macrophages

For the assessment of glucose uptake, we opted to use ^{3}H-2-deoxyglucose, rather than ^{18}F-FDG, because of the long half-life of ^{3}H. Macrophage stimulation by LPS resulted in a 2.5-fold increase in ^{3}H-2-deoxyglucose uptake (Fig. 2A). In contrast, neither M1 nor M2 polarized macrophages showed any significant increase in ^{3}H-2-deoxyglucose uptake. The 2 rate-limiting steps in the intracellular accumulation of deoxyglucose are facilitated transport by glucose transporters and intracellular trapping through phosphorylation by hexokinases (19). We therefore evaluated by qRT-PCR the expression of Glut-1, the major glucose transporter isoform involved in glucose uptake by macrophages (13), and the expression of the hexokinase isoforms, Hk-1 and Hk-2. Consistent with the enhanced ^{3}H-2-deoxyglucose uptake in M_{LPS} macrophages, LPS resulted in a 5.7-fold increase in Glut-1 expression (Fig. 2B). Neither M1 nor M2 polarization affected Glut-1 expression in peritoneal macrophages. In agreement with these results, we also found in M_{LPS} macrophages a 3.4- and 4.1-fold increase in expression of Hk-1 and Hk-2, respectively, compared with M0

macrophages (Figs. 2C and 2D). In contrast, Hk-1 and Hk-2 induction was significantly less pronounced in both M1 and M2 polarized macrophages. M2 polarized macrophages showed a 1.9-fold increase in Hk-1 and a 2.5-fold in Hk-2 expression, compared with M0 macrophages. M1 polarization resulted in a 2-fold induction of Hk-2 but in no significant induction of Hk-1 (Figs. 2C and 2D).

Distinct Mitochondrial Respiratory Profiles During Macrophage Polarization

Activation of immune cells is associated with enhanced energy demand (20). Therefore, we evaluated whether M1 and M2 polarized macrophages were able to use oxidative phosphorylation as a more efficient and alternative mechanism for ATP generation. To this end, we measured resting OCR and the mitochondrial respiratory profiles of M0, M1, M2, and polarized macrophages (Fig. 3). Rotenone-insensitive (i.e., residual cellular) OCR, reflecting oxygen consumption by nonmitochondrial sources, was similar between all 4 groups and thus independent of the polarization state of the macrophages (Fig. 3). However, basal mitochondrial respiration was significantly lower in M_{LPS} macrophages than in M0 macrophages (Supplemental Fig. 2A). Basal OCR was not significantly different between M0 macrophages with either M1 or M2 polarized cells. OCR attributable to ATP production (Supplemental Fig. 2B) and proton leak (Supplemental Fig. 2C) was also comparable among the groups without any statistically significant difference. Interestingly, treatment of M0, M_{LPS}, or M1 polarized macrophages with FCCP failed to increase OCR, compared with the basal level (Fig. 3), consistent with a lack of any significant spare respiratory capacity in these cells (Supplemental Figs. 2D and 2E). In stark contrast, M2 polarized macrophages increased their OCR to more than 2.2-fold of the basal level in the presence of FCCP (Fig. 3), demonstrating that alternatively activated macrophages developed a significant spare respiratory capacity (Supplemental Fig. 2D). Consistent with this finding, the maximal respiratory capacity of M2 polarized macrophages was also significantly higher than that of M_{LPS} and M1 polarized macrophages (Supplemental Fig. 2E).

Next, we examined the basal ECAR-to-OCR ratio to evaluate the extent by which macrophages use glycolysis as compared with oxidative phosphorylation to meet their energy demand. The ECAR-to-OCR ratio was significantly higher in M_{LPS} macrophages than in M0, M1, and M2 polarized macrophages (Fig. 4), demonstrating that LPS stimulation shifts the macrophages' energy supply from mitochondrial ATP production toward glycolysis, resulting in extracellular acidification.

Mitochondrial Biogenesis in M2 Polarized Macrophages

We quantified the mitochondrial content of polarized macrophages, as a major determinant of spare respiratory capacity. As shown in Figure 5A, mtDNA copy number was 4.6-fold higher in M2 polarized macrophages than in M0 macrophages,

RGB

FIGURE 2. Macrophage polarization and glucose utilization. Glucose uptake and RNA expression of genes involved in intracellular trapping of ^{3}H-2-deoxyglucose is enhanced in M_{LPS} macrophages. Inflammatory polarization of macrophages by LPS (M_{LPS}), unlike IFN-γ plus TNF-α (M1), markedly enhances ^{3}H-2-deoxyglucose uptake (A), which is associated with overexpression of Glut-1 (B), Hk-1 (C), and Hk-2 (D). M2 polarization has no effect on glucose uptake or expression of Glut-1. Modest increase is present in Hk-1 and Hk-2 expression in M2 and Hk-2 expression in M1 polarized macrophages without concomitant increase in Glut-1 expression or ^{3}H-2-deoxyglucose uptake (n = 5 for deoxyglucose uptake and n = 3 for gene expression experiments). mRNA = messenger RNA.

FIGURE 3. Mitochondrial bioenergetics and macrophage polarization. Real-time analysis of OCR demonstrates markedly different respiratory profiles among polarized murine peritoneal macrophages at baseline and after incubation with specific mitochondrial inhibitors. Basal mitochondrial respiration is significantly lower in M_{LPS} than in nonpolarized macrophages. Spare respiratory capacity is negligible in nonpolarized and classically polarized (M1 and M_{LPS}) macrophages. On the other hand, OCR reaches to about 2.2-fold of basal level in M2 polarized macrophages in presence of FCCP, indicating significant spare respiratory capacity of these cells. Consistently, maximal respiratory capacity of M2 polarized macrophages is also significantly higher in M2 than in classically (M1 and M_{LPS}) polarized macrophages ($n = 7$).

indicating that mitochondrial biogenesis is activated during alternative macrophage polarization. Increased mtDNA copy number in M2 macrophages was associated with a 1.7-fold increase in the expression of *Tfam,* an essential transcription factor in mtDNA replication (*21*), and a 2.4-fold increase in the expression of *Cox-1,* the gene encoding cytochrome c oxidase subunit I (Figs. 5B and 5C). There was no significant difference in the expression of *Tfam* or *Cox-1* and mitochondrial content of M0 and M1 polarized macrophages. Despite the significantly lower basal mitochondrial respiration (Supplemental Fig. 2A), mitochondrial content of M_{LPS} macrophages was not lower than that of M0 macrophages (Fig. 5A), indicating that a functional defect underlies LPS-induced suppression of oxidative phosphorylation. Additionally, the expression of both *Tfam* and *Cox-1* was significantly higher in M_{LPS} macrophages than in nonpolarized macrophages, suggesting defective mitochondrial biogenesis induced by LPS.

DISCUSSION

The goal of this study was to determine the metabolic profiles of macrophages polarized into distinct polarization states. We found that macrophages, depending on the stimulus and their polarization state, alter their reliance on glycolysis versus mitochondrial respiration for energy production.

Microvascular occlusion and the rapid recruitment of inflammatory cells typically produce a hypoxic microenvironment in sites of inflammation due to the increased tissue cellularity, which exceeds the tissue's angiogenic capacity (*22*). Atherosclerotic plaques in both human and animal models contain hypoxic areas, which may contribute to the progression of lesions and expansion of the necrotic core (*23,24*). Macrophages are well equipped with a metabolic arsenal to survive in hypoxic environments (*25*),

which is activated, at least in part, by overexpression of hypoxia-inducible factors 1 and 2 (*22*). Relying on glycolysis rather than mitochondria for energy production allows macrophages to switch to anaerobic metabolism. It was therefore assumed that activated macrophages would increase their glucose uptake, which prompted investigators to use glucose uptake as a noninvasive approach for imaging macrophage activation in atherosclerosis. The availability and safety of ^{18}F-FDG for human use have allowed for early evaluation of this tracer in human vascular diseases (*1,5,10,26*). ^{18}F-FDG PET imaging of carotid atherosclerotic disease is reproducible (*27*), with a high inter- and intrareader agreement (*28,29*), and has been reported to correlate with the macrophage content of plaques and the risk of future vascular events (*28,30–32*), suggesting that it may be used to monitor disease progression and predict adverse outcome and the efficacy of therapeutic interventions (*10,19*). ^{18}F-FDG PET imaging of coronary arteries is technically more challenging because of the high myocardial glucose uptake, cardiac motion, and small caliber of the vessels with regard to the low resolution of PET. However, it has been shown that high ^{18}F-FDG uptake can identify left main coronary artery culprit lesions in acute coronary syndromes (*26*). On the other hand, there are also both animal and human studies demonstrating a lack of correlation between ^{18}F-FDG uptake and macrophage content of atherosclerotic lesions (*4,9*). These controversial data have been a major obstacle in the translation of ^{18}F-FDG PET imaging into the clinical practice. We hypothesized that the diversity of macrophage activation pathways may explain some of these conflicting data and therefore determined the impact of macrophage polarization on glucose uptake and oxidative phosphorylation.

Microenvironmental cues (e.g., cytokines and intercellular or extracellular interactions) allow macrophages to undergo different activation programs, which range from proinflammatory (M1 or classic polarization) to antiinflammatory (M2 or alternative polarization) phenotypes (*2*). IFN-γ and LPS either alone or in combination with other inflammatory cytokines—for example, TNF-α—are the most widely used stimuli to induce M1 macrophage polarization, characterized by high expression of proinflammatory cytokines, such as IL-1β, IL-6, IL-12, and TNF-α (*2*). Growth factors, such as granulocyte macrophage colony-stimulating factor, can also induce M1 macrophage polarization (*5*). M2 polarization in macrophages is induced ex vivo using cytokines, such as IL-4,
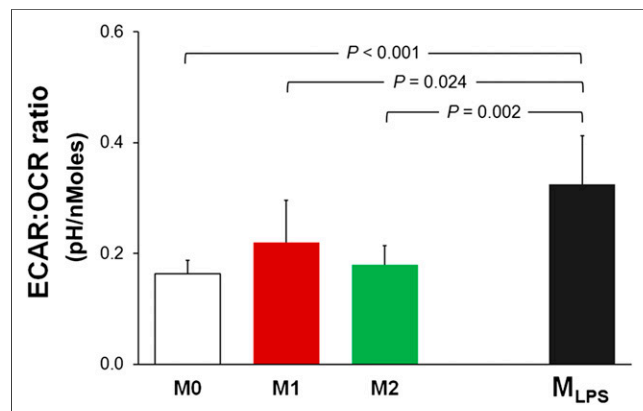
FIGURE 4. Glycolysis vs. oxidative phosphorylation in polarized macrophages. Basal ECAR-to-OCR ratio is significantly higher in M_{LPS} macrophages than in M0, M1, and M2 polarized macrophages, demonstrating that LPS induced shift away from oxidative phosphorylation toward glycolysis ($n = 7$).
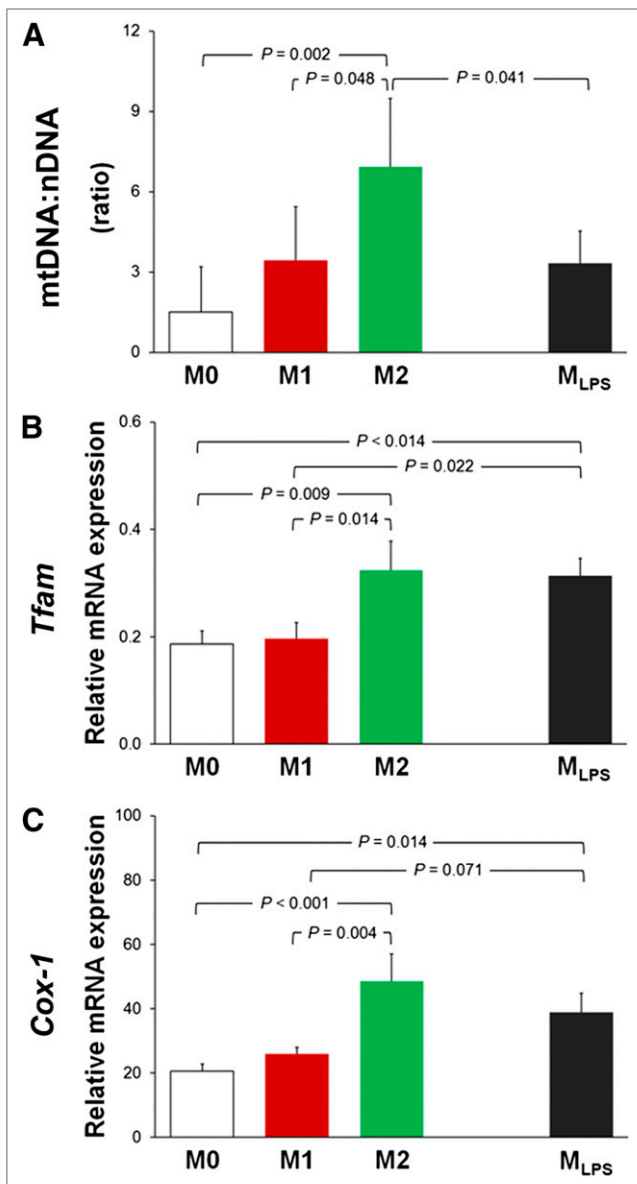
FIGURE 5. Mitochondrial biogenesis and macrophage polarization. Mitochondrial content and RNA expression of genes involved in mitochondrial biogenesis and oxidative phosphorylation is significantly enhanced in M2 polarized murine peritoneal macrophages. M2 polarization promotes mitochondrial biogenesis, as shown by increased mitochondrial DNA copy number (mtDNA-to-nDNA ratio) (A) and expression of *Tfam* (B), and *Cox-1* (C). No significant difference exists in expression of *Tfam* and *Cox-1* or mitochondrial content of M0 and M1 polarized macrophages. LPS treatment induced expression of both *Tfam* and *Cox-1,* but this was not associated with significant increase in mitochondrial content of M_{LPS} macrophages ($n = 5$ for mtDNA copy number and $n = 3$ for gene expression experiments). mRNA = messenger RNA.

tion of plaque macrophages toward the alternative polarization phenotype (*35*). Therefore, monitoring alterations in the polarization state of macrophages, in addition to the tracking of circulating monocyte recruitment and macrophage content of plaques, may help to accurately identify vulnerable lesions and determine the dynamics of plaque progression or regression.

^{18}F-FDG PET imaging of atherosclerosis relies on the detection of enhanced glucose uptake by activated macrophages. However, recent experimental data obtained ex vivo have been controversial. Some studies demonstrated unchanged glucose uptake by inflammatory activation of macrophages (IFN-γ alone or in combination with TNF-α, IL-1β) (*13*). Others showed enhanced glucose uptake by classic (combination of TNF-α, IL-1β, IFN-γ, and granulocyte macrophage colony-stimulating factor), but not alternative (IL-4 and IL-13), macrophage polarization (*36*) and increased glucose uptake by both M1 (cotreatment with IFN-γ and LPS) and M2 (IL-4) polarized macrophages (*37*). Different sources of macrophages (i.e., human monocyte–derived macrophages in the first (*13*) and murine bone marrow–derived macrophages in the latter 2 studies (*36–38*)) and the use of different polarization agents may have contributed to these conflicting data. Here, we demonstrated that glucose uptake is enhanced by LPS but not another well-established inflammatory polarization protocol—that is, IFN-γ plus TNF-α. Increased glucose uptake by M_{LPS} was associated with overexpression of *Glut-1* as well as *Hk-1* and *Hk-2,* which are critical in transmembrane transport and intracellular trapping of 2-deoxyglucose. These findings demonstrate that enhanced glucose uptake depends on the specific agents activating macrophages—for example, endotoxin—and is not an indispensible component of polarization into an inflammatory state. In this study, we chose LPS as one of the most accepted agents to induce inflammatory macrophage polarization ex vivo. There is evidence that even a low level of endotoxemia may trigger or accelerate atherosclerosis by accentuating the production of proinflammatory chemokines and cytokines, adhesion molecules, and reactive oxygen species (*39*). Other stimulatory agents in a plaque microenvironment—including cytokines and growth factors, which may enhance macrophage glucose uptake—remain to be determined.

M2 polarization of macrophages was associated with the activation of mitochondrial biogenesis as shown by marked overexpression of *Tfam* and *Cox-1,* an increase in mitochondrial content of the macrophages, and the acquisition of a significant spare respiratory capacity, which allowed M2 polarized macrophages to reach a maximal OCR of more than double their basal respiration. Increasing the spare respiratory capacity has been proposed to improve the bioenergetic stability of cells by decreasing their dependence on energetically less productive glycolysis and by increasing the range of potential substrates (e.g., lipids and amino acids) (*15,40*). This may provide M2 macrophages with a survival advantage during the resolution of inflammation, when proglycolytic signaling mechanisms are fading away (*40*), a deleterious condition for cells that are predominantly dependent on glycolysis, such as classically polarized macrophages. We can speculate that the lack of a significant respiratory capacity in classically polarized macrophages may contribute to the preferential death of these macrophage subsets during the resolution phase of inflammation and thus the development of a predominantly M2-skewed milieu, diminishing inflammation. Therefore, the impact of these divergent metabolic profiles of polarized macrophages may extend well beyond imaging applications, because they may play significant roles in the etiology of atherosclerotic plaques.

IL-10, and IL-13, and growth factors, such as monocyte colony-stimulating factor (*2*). These cells are characterized by the production of antiinflammatory mediators, and they contribute to the resolution of inflammation and tissue repair (*2*). Both M1 and M2 macrophages have been identified in human (*33*) and mouse (*34*) atherosclerotic lesions. Recent data suggest that improved metabolic profile (e.g., reduction of hyperlipidemia and hyperglycemia) induces polariza-

RGB

CONCLUSION

Our data demonstrate that enhanced glucose uptake is not an intrinsic feature of inflammatory activation of macrophages but appears to be induced by selected stimuli, such as LPS. We also showed that M2 macrophage polarization induces mitochondrial biogenesis, resulting in the acquisition of a significant spare respiratory capacity, which may provide these cells with the necessary bioenergetic flexibility to survive for long periods in a hostile environment. Our identification of a wide metabolic diversity among polarized macrophages has profound implications for the interpretation of biologic correlates obtained in patients with atherosclerosis by in vivo imaging approaches (e.g., ^{18}F-FDG PET) that target alterations in the metabolic pathways of macrophages, as markers of disease progression/regression and as measures of response to therapy.

DISCLOSURE

ACKNOWLEDGMENT

REFERNCES

1. Tavakoli S, Sadeghi MM. Imaging of vascular biology in the heart. *Curr Cardiovasc Imaging Rep.* 2009;2:40–49.
2. Tavakoli S, Asmis R. Reactive oxygen species and thiol redox signaling in the macrophage biology of atherosclerosis. *Antioxid Redox Signal.* 2012;17:1785–1795.
3. Rabbani R, Topol EJ. Strategies to achieve coronary arterial plaque stabilization. *Cardiovasc Res.* 1999;41:402–417.
4. Myers KS, Rudd JH, Hailman EP, et al. Correlation between arterial FDG uptake and biomarkers in peripheral artery disease. *JACC Cardiovasc Imaging.* 2012;5:38–45.
5. Figueroa AL, Subramanian SS, Cury RC, et al. Distribution of inflammation within carotid atherosclerotic plaques with high-risk morphological features: a comparison between positron emission tomography activity, plaque morphology, and histopathology. *Circ Cardiovasc Imaging.* 2012;5:69–77.
6. Fayad ZA, Mani V, Woodward M, et al. Safety and efficacy of dalcetrapib on atherosclerotic disease using novel non-invasive multimodality imaging (dal-PLAQUE): a randomised clinical trial. *Lancet.* 2011;378:1547–1559.
7. Choi YS, Youn HJ, Chung WB, et al. Uptake of F-18 FDG and ultrasound analysis of carotid plaque. *J Nucl Cardiol.* 2011;18:267–272.
8. Wu YW, Kao HL, Huang CL, et al. The effects of 3-month atorvastatin therapy on arterial inflammation, calcification, abdominal adipose tissue and circulating biomarkers. *Eur J Nucl Med Mol Imaging.* 2012;39:399–407.
9. Laurberg JM, Olsen AK, Hansen SB, et al. Imaging of vulnerable atherosclerotic plaques with FDG-microPET: no FDG accumulation. *Atherosclerosis.* 2007;192:275–282.
10. Rosenbaum D, Millon A, Fayad ZA. Molecular imaging in atherosclerosis: FDG PET. *Curr Atheroscler Rep.* 2012;14:429–437.
11. Gautier EL, Huby T, Witztum JL, et al. Macrophage apoptosis exerts divergent effects on atherogenesis as a function of lesion stage. *Circulation.* 2009;119:1795–1804.
12. Tabas I. Macrophage death and defective inflammation resolution in atherosclerosis. *Nat Rev Immunol.* 2010;10:36–46.
13. Folco EJ, Sheikine Y, Rocha VZ, et al. Hypoxia but not inflammation augments glucose uptake in human macrophages: implications for imaging atherosclerosis with [18]fluorine-labeled 2-deoxy-D-glucose positron emission tomography. *J Am Coll Cardiol.* 2011;58:603–614.
14. Qiao M, Zhao Q, Lee CF, et al. Thiol oxidative stress induced by metabolic disorders amplifies macrophage chemotactic responses and accelerates atherogenesis and kidney injury in LDL receptor-deficient mice. *Arterioscler Thromb Vasc Biol.* 2009;29:1779–1786.
15. Nicholls DG, Darley-Usmar VM, Wu M, Jensen PB, Rogers GW, Ferrick DA. Bioenergetic profile experiment using C2C12 myoblast cells. *J Vis Exp.* 2010;46:2511.
16. Guo W, Jiang L, Bhasin S, Khan SM, Swerdlow RH. DNA extraction procedures meaningfully influence qPCR-based mtDNA copy number determination. *Mitochondrion.* 2009;9:261–265.
17. Pena OM, Pistolic J, Raj D, Fjell CD, Hancock RE. Endotoxin tolerance represents a distinctive state of alternative polarization (M2) in human mononuclear cells. *J Immunol.* 2011;186:7243–7254.
18. Porta C, Rimoldi M, Raes G, et al. Tolerance and M2 (alternative) macrophage polarization are related processes orchestrated by p50 nuclear factor kappaB. *Proc Natl Acad Sci USA.* 2009;106:14978–14983.
19. Aloj L, Caraco C, Jagoda E, Eckelman WC, Neumann RD. Glut-1 and hexokinase expression: relationship with 2-fluoro-2-deoxy-D-glucose uptake in A431 and T47D cells in culture. *Cancer Res.* 1999;59:4709–4714.
20. Través PG, de Atauri P, Marin S, et al. Relevance of the MEK/ERK signaling pathway in the metabolism of activated macrophages: a metabolomic approach. *J Immunol.* 2012;188:1402–1410.
21. Kelly DP, Scarpulla RC. Transcriptional regulatory circuits controlling mitochondrial biogenesis and function. *Genes Dev.* 2004;18:357–368.
22. Murdoch C, Muthana M, Lewis CE. Hypoxia regulates macrophage functions in inflammation. *J Immunol.* 2005;175:6257–6263.
23. Parathath S, Mick SL, Feig JE, et al. Hypoxia is present in murine atherosclerotic plaques and has multiple adverse effects on macrophage lipid metabolism. *Circ Res.* 2011;109:1141–1152.
24. Vink A, Schoneveld AH, Lamers D, et al. HIF-1 alpha expression is associated with an atheromatous inflammatory plaque phenotype and upregulated in activated macrophages. *Atherosclerosis.* 2007;195:e69–e75.
25. Cramer T, Yamanishi Y, Clausen BE, et al. HIF-1alpha is essential for myeloid cell-mediated inflammation. *Cell.* 2003;112:645–657.
26. Rogers IS, Nasir K, Figueroa AL, et al. Feasibility of FDG imaging of the coronary arteries: comparison between acute coronary syndrome and stable angina. *JACC Cardiovasc Imaging.* 2010;3:388–397.
27. Rudd JH, Myers KS, Bansilal S, et al. [18]Fluorodeoxyglucose positron emission tomography imaging of atherosclerotic plaque inflammation is highly reproducible: implications for atherosclerosis therapy trials. *J Am Coll Cardiol.* 2007;50:892–896.
28. Rominger A, Saam T, Wolpers S, et al. ^{18}F-FDG PET/CT identifies patients at risk for future vascular events in an otherwise asymptomatic cohort with neoplastic disease. *J Nucl Med.* 2009;50:1611–1620.
29. Rudd JH, Myers KS, Bansilal S, et al. Atherosclerosis inflammation imaging with ^{18}F-FDG PET: carotid, iliac, and femoral uptake reproducibility, quantification methods, and recommendations. *J Nucl Med.* 2008;49:871–878.
30. Tawakol A, Migrino RQ, Bashian GG, et al. In vivo ^{18}F-fluorodeoxyglucose positron emission tomography imaging provides a noninvasive measure of carotid plaque inflammation in patients. *J Am Coll Cardiol.* 2006;48:1818–1824.
31. Rudd JH, Warburton EA, Fryer TD, et al. Imaging atherosclerotic plaque inflammation with [^{18}F]-fluorodeoxyglucose positron emission tomography. *Circulation.* 2002;105:2708–2711.
32. Marnane M, Merwick A, Sheehan OC, et al. Carotid plaque inflammation on ^{18}F-fluorodeoxyglucose positron emission tomography predicts early stroke recurrence. *Ann Neurol.* 2012;71:709–718.
33. Waldo SW, Li Y, Buono C, et al. Heterogeneity of human macrophages in culture and in atherosclerotic plaques. *Am J Pathol.* 2008;172:1112–1126.
34. Khallou-Laschet J, Varthaman A, Fornasa G, et al. Macrophage plasticity in experimental atherosclerosis. *PLoS ONE.* 2010;5:e8852.
35. Parathath S, Grauer L, Huang LS, et al. Diabetes adversely affects macrophages during atherosclerotic plaque regression in mice. *Diabetes.* 2011;60:1759–1769.
36. Tawakol A, Rudd J, Fayad Z, Bosca L. Classical but not innate activation augments 2-deoxy-D-glucose uptake in macrophages: implications for atherosclerosis imaging [abstract]. *J Nucl Med.* 2012;53(suppl):464.
37. Vats D, Mukundan L, Odegaard JI, et al. Oxidative metabolism and PGC-1beta attenuate macrophage-mediated inflammation. *Cell Metab.* 2006;4:13–24.
38. Tavakoli S, Razavian M, Zhang J, et al. Matrix metalloproteinase activation predicts amelioration of remodeling after dietary modification in injured arteries. *Arterioscler Thromb Vasc Biol.* 2011;31:102–109.
39. Stoll LL, Denning GM, Weintraub NL. Potential role of endotoxin as a proinflammatory mediator of atherosclerosis. *Arterioscler Thromb Vasc Biol.* 2004;24:2227–2236.
40. van der Windt GJ, Everts B, Chang CH, et al. Mitochondrial respiratory capacity is a critical regulator of CD8+ T cell memory development. *Immunity.* 2012;36:68–78.